13th International Symposium on Turbulence and Shear Flow Phenomena (TSFP13)
Montreal, Canada, June 25–28, 2024

IDENTIFICATION OF COHERENT STRUCTURES IN THE WAKE OF A ROTATING WHEEL USING HIGH-SPEED PIV MEASUREMENTS AND THE SPECTRAL POD METHOD

Ivan Joksimović
Institute of Fluid Mechanics and Aerodynamics
Technical University of Darmstadt
Peter-Grünberg-Straße 10, D-64287 Darmstadt
joksimovic@sla.tu-darmstadt.de

Philipp Brockmann
Institute of Fluid Mechanics and Aerodynamics
Technical University of Darmstadt
Peter-Grünberg-Straße 10, D-64287 Darmstadt
brockmann@sla.tu-darmstadt.de

Jeanette Hussong
Institute of Fluid Mechanics and Aerodynamics
Technical University of Darmstadt
Peter-Grünberg-Straße 10, D-64287 Darmstadt
brockmann@sla.tu-darmstadt.de

Suad Jakirlić
Institute of Fluid Mechanics and Aerodynamics
Technical University of Darmstadt
Peter-Grünberg-Straße 10, D-64287 Darmstadt
jakirlic@sla.tu-darmstadt.de

ABSTRACT

The present work demonstrates how the Spectral-Proper-Orthogonal-Decomposition (SPOD) algorithm can be used to isolate coherent structures and understand the dominant mechanisms in the wake of a rotating car wheel, taking into account rim details and a groove-like tire profile. The source data, consisting of the 2D velocity field, was provided by the HighSpeed PIV measurements of the near-ground wake zone. The experimental case consists of the full-scale (1:1) notchback configuration of the well-known 'DrivAer' vehicle model, with rotating wheels. The results show that the near-ground wake zone is dominated by two important mechanisms: first, the rotation and ventilation effects of the wheel itself, with an oscillation frequency corresponding to the wheel rotation frequency. The other dominant mechanism is pulsations associated with the large-scale shear phenomena present in the ring-vortex pairs around the wheels. The present analysis provides a better insight into the dynamics of coherent structures in the wheel region.

INTRODUCTION

Recent trends in the development of electric vehicles impose increasingly strict constraints on vehicle aerodynamics, especially from the point of view of its optimization, e.g. minimization of drag. This stimulates an intense research activity aimed at identifying and understanding the relevant aerodynamic phenomena. This trend becomes increasingly important in the wheel area, where the drag induced by the ventilation effect of the rotating wheel reaches approximately 25% of the total drag. Therefore, the identification and understanding of relevant aerodynamic mechanisms in the rotating wheel zone becomes a high priority task in the search for minimizing the total vehicle drag.

Until now, statistical techniques have been the primary method for analyzing transient, turbulent flow in the vehicle wake. On the negative side, such an approach filters out substantial information about the flow from the domain, thus demotivating the usually high cost of experiment/simulation. In recent years, to mitigate this problem, modal analysis techniques such as POD (Proper-Orthogonal-Decomposition) and DMD (Dynamic Mode Decomposition) have been increasingly used, as exemplified in Mrosek & Othmer (2019) and Matsumoto *et al.* (2019), to isolate the coherent structures from the flow field and to obtain additional information about their dynamics.

Recently, the algorithm of Spectral-Proper-Orthogonal-Decomposition (SPOD), by Schmidt & Colonius (2020), has emerged as an interesting alternative, isolating the coherent structures whose temporal dynamic properties are bound to the oscillation at a certain frequency. In this way, a procedure similar to the spatially applied *Discrete Fourier Transform* (DFT) has been obtained. This algorithm has proven to be a viable alternative to the aforementioned POD and DMD, with the main advantages being the increased robustness in overcoming the problems caused by the presence of noise, and the ease of interpretation of the results.

THEORETICAL BACKGROUND OF THE SPOD ALGORITHM

The complete algorithm for performing the SPOD analysis has been discussed in detail by Schmidt & Colonius (2020). At this point, is suffices to say that the SPOD is based on finding spatially orthogonal structures in the phase space, created by applying the time DFT to the chunked data matrix, containing snapshots of the velocity field. As a result, coherent structures, representing band-filtered pulsations of the velocity field are isolated from the data, enabling a deeper understanding of the underlying flow dynamics.

Suppose that that the state of the observed system, denoted with $q(\mathbf{x},t)$ is captured in M discrete locations, indexed by i in the domain. If the discrete time of the observation is indexed with j, the data can be arranged in the so-called *snapshot* vector $q_{i,j}$. Furthermore, if N temporally equidistant snapshots of the system are made, the data matrix for a single measurement k has the following form:

$$Q^k_{M\times N} = \left[q^k_{i,1}, q^k_{i,2}, ..., q^k_{i,j}, .., q^k_{i,N}\right] \tag{1}$$

Finally, when a total of K of measurements have been taken, the summary data matrix will take the form of

$$\begin{aligned} Q_{M\times N\times K} &= \left[Q^1, Q^2, ..., Q^k, ..., Q^K\right] \\ &= \left[q_{i,j,1}, q_{i,j,2}, \cdots, q_{i,j,k}, \cdots, q_{i,j,K}\right] \end{aligned} \tag{2}$$

At this point, it is important to make a first assumption about the state of the system, i.e., that the observed system is statistically stationary, i.e., that all statistical moments of $q(\mathbf{x},t)$ remain unchanged regardless of the observation. In addition, it is assumed that the observed statistics can also be characterized as repeatable, despite the fact that the observed variable may be random, as is the case with turbulence. With this in mind, mean-padding of Q is performed to eliminate the DC component from the measurements, leaving only the AC component for further analysis.

Assuming statistical stationarity, the row-wise DFT algorithm is performed for each point in the domain and for each measurement in the batch, yielding a frequency-coded data matrix:

$$\hat{Q}_{M\times N_{FFT}\times K} = \left[\hat{q}_{i,j,1}, \hat{q}_{i,j,2}, ...\hat{q}_{i,j,k}, ..., \hat{q}_{i,N_{FFT},K}\right] \tag{3}$$

Each element of the matrix thus encodes the pulsation dynamics at point i, represented by the j-th frequency in the spectrum taken from measurement k. A total of N_{FFT} frequencies is the result of possible techniques to improve resolution and spectral leakage, such as windowing and zero padding.

The final step is to isolate spectrally correlated structures, i.e., spatial structures whose pulsation dynamics is tied to the same frequency. In the case of the hypothetical noise-free measurements, the previous step with the row-wise DFT transformation would be sufficient to isolate this signal. However, in the case of real data, especially from experimental measurements, the source data is often corrupted by some level of noise, resulting in highly scattered structures as well as low confidence in the amplitude of the detected pulsations. This is one of the main reasons for making a series of multiple measurements, where the goal is to find those structures (modes) that are repeated in each measurement, thus increasing the confidence and smoothness of the result. For this purpose, a POD-like procedure is performed in the following way:

For each of the calculated frequencies, j, a so-called block matrix is isolated from the main data-matrix $\hat{Q}$:

$$\hat{Q}_{M\times K} = \left[\hat{q}_{i,j,1}, \hat{q}_{i,j,2}, ..., \hat{q}_{i,j,K}\right] \tag{4}$$

Finally, the following eigendecomposition is performed:

$$\hat{\mathbf{Q}}_f \hat{\mathbf{Q}}_f^{\dagger} \Psi_f = \Lambda_f \Psi_f \tag{5}$$

Two important pieces of information are extracted from the equation 5: First, a diagonal matrix Λ_f containing K non-zero eigenvalues $\lambda_{f,k}$, and the eigenvectors (also called 'modes') $\Psi_{f,k}$ contained in the columns of the matrix Ψ_f. The physical interpretation of the respective modes and eigenvalues is straightforward: since the modes $\Psi_{f,k}$ are mutually orthogonal, and since the equation 5 is equivalent to the SVD (Singular-Value-Decomposition) of $\hat{\mathbf{Q}}_f$, each eigenvalue will represent a variance contained in the mode $\Psi_{f,k}$. If the eigendecomposition **??** is performed for each frequency, one can also compute the total power-spectral density PSD for each frequency in the domain as:

$$PSD = \left[\sum_{i=1}^{N_{blocks}} \lambda_i^1, \sum_{i=1}^{N_{blocks}} \lambda_i^2, ..., \sum_{i=1}^{N_{blocks}} \lambda_i^k, ..., \sum_{i=1}^{N_{blocks}} \lambda_i^{N_{FFT}}\right] \tag{6}$$

where N_{blocks} represents the number of blocks, used in chunking of the data-matrix, and λ_i^k the eigenvalue associated with the k-th frequency of the i-th block.

The reconstruction of the original pulsation field can also be carried out if all the modes are known, such as the following

$$\mathbf{u}'(\mathbf{x},t) = \sum_k \int_{-\infty}^{+\infty} \hat{a}_{k,f}\, \hat{\psi}_{k,f}(\mathbf{x}) e^{i2\pi f} df \tag{7}$$

where $\hat{a}_{k,f}$ represents the amplitude of the k-th mode at frequency f. For this work however, a far more important feature is to isolate those pulsations whose dynamics is bound to the specific frequency of interest, f. This is done using:

$$\mathbf{u}'_f(\mathbf{x},t) = \sum_k \hat{a}_{k,f}\, \hat{\psi}_{k,f}(\mathbf{x}) e^{i2\pi f t} \tag{8}$$

EXPERIMENTAL DETAILS

As already mentioned, the source data for the algorithm are provided by measurements performed in the wind tunnel of the FKFS Institute in Stuttgart, Germany, as part of the FAT project: *Characterization and simulation of flow around wheels with realistic tire deformations* (in German: *Charakterisierung und Simulation der Radumströmung bei realer Reifendeformation*). Figure 1 visualizes the experimental setup with key components, with the well-known 'DrivAer' vehicle mock-up in the center. The currently adopted DrivAer model configuration is the notchback variant with flat underbody (the originally designed DrivAer model is by **?**). As you can see, the measurement zone is located near the left front wheel, while the measurement plane can be positioned between $35-90$ mm above the ground. For this work, we will focus on the 2D measurements positioned 35 mm above the ground. From the raw data, a batch of four measurements can be reconstructed, where each measurement contains 472 snapshots of the 2D velocity field. From each measurement, three blocks with 50% temporal overlap can be created, resulting in a total of twelve data blocks. The sampling period per measurement is 1.892 $[s]$.

RESULTS AND DISCUSSION

The mean-field statistics resulting from averaging all snapshots of the velocity field are shown in Figures 2 and 3. The observation window is viewed from the ground plane, while the tire contour with grooves is shown in the background. As can be seen in Figure 2, a well-defined wake develops direkt around the tire, with a shear zone separating the free-flow. Figure 3 shows the average intensity of the velocity field pulsations in the observation window. As can be seen, the shear zone is dominated by the fluctuations whose amplitude is in the range of 20% to 30% of the free stream velocity. Due to this elevated intensity, it is expected that some large-scale unsteady physical mechanisms can be reconstructed from the flow data. As can be seen, the elevated fluctuation intensities in the upper left and upper right corners are due to the measurement noise and do not have any coherence nor do they represent any physical phenomena. Once the statistical analysis is complete, the analysis of the SPOD results can begin. Before analyzing the results, i.e. the dynamics of coherent structures in the shear zone, certain assumptions have to be made about the expected phenomena in the flow field. Since SPOD isolates the coherent structures based on their oscillation frequency, one can expect at least one mechanism in the flow field to be bound to the rotation frequency of the wheel, $f = U_\infty/(2\pi D_{wheel})$, where U_∞ is the car velocity and D_{wheel} is the wheel diameter. In addition, since a wheel has five spokes (representing the geometric characteristics of the rim), the frequency based on spoke ventilation can also be formed as $f_{spoke} = 5f_{wheel} = 5U_\infty/(2\pi D_{wheel})$. Finally, the third and fourth characteristic frequencies in the flow field can be formed based on either the car length or the car width L_{car}, $f_{car} = U_\infty/L_{car}$. The latter would represent the frequency of some large scale shear phenomena caused by the instabilities in the car wake. Based on the geometric and boundary conditions, these four characteristic frequencies are given in Table 1.

Table 1. Characteristic times and frequencies

Description	Frequency $[Hz]$
Flow over car length	6.02
Flow over car width	15.19
Wheel rotation	14.04
Rotation of one spoke	70.17

Figure 4 shows the SPOD spectrum discussed in equation 6, with three leading eigenvalues in the frequency range up to 120 Hz. Additionally, the Power-Spectral-Density (sum of all eigenvalues per frequency) is plotted as to give the insight into the energy distribution at different frequencies. Based on the leading eigenvalues (blue line), there is a single over-dominant phenomenon at $f \approx 70\ Hz$, which is recalled to be the spoke rotation frequency related to the ventilation moment. This pulsation represents ≈ 4 % of the total turbulent kinetic energy in the system, which means that, as expected, most of the dominant phenomena in the observation zone near the ground represent a ventilation phenomenon. The corresponding coherent structure is visualized in Figure 4. Here the equation 8 with only the leading SPOD mode is used to visualize the pulsations of the velocity field occurring at $f \approx 70\ Hz$. As can be seen, contrasting red and blue zones mark the spots of high local pulsation intensity, which are arranged in a chain of *pulsation bubbles*, located at the edge of the shear zone. The maximum amplitude reaches about $\approx 4.73\ m/s$, which, together with the large spatial range of the pulsation, accounts for the predominance of this phenomenon in the field of observation. The relatively narrow confidence interval with respect to the maximum amplitude can be explained by the high signal-to-noise ratio in the actual case.

The second most dominant pulsation in terms of energy contained is identified at the frequency of about $f \approx 6 - 8\ Hz$, already deduced in the last section. This means that the SPOD procedure has successfully managed to capture the aforementioned large scale shear phenomena, which seems to be spatially positioned towards the centerline of the car. Interestingly, this coherent structure does not seem to be located directly in the shear zone, in the region of high intensity pulsations (see Figure 3), but rather more inwardly, in the wake. As previously deduced, this particular structure may be associated with the shear phenomena in the car wake due to the matching frequency, see Table 1, or with some other phenomena present in the ring vortices developing in the wheel wake.

The third dominant peak in the SPOD spectrum is located at the frequency $f \approx 14\ Hz$, which corresponds exactly to the rotation frequency of the wheel according to Table 1. In the spatial visualization of the mode (Figure 7) it can be seen that the span of the pulsation bubble is aligned with the mean shear zone. The relatively wide confidence interval for this particular mode can be explained by the low signal-to-noise ratio, which is also visible in the SPOD spectrum, where there is a much wider separation between the eigenvalues of the second (red line) and third (green line) SPOD modes at this frequency. This can also be seen in the mode reconstruction itself, where the spatial representation of the coherent structure clearly shows the presence of some noise.

Finally, let us examine the fourth dominant peak of the SPOD spectrum, with a frequency of $f \approx 32\ Hz$, which does not coincide with any of the frequencies listed in Table 1. The identification of the relevant phenomena according to the characteristic frequency doesn't seem to be easy in this particular case, although it can be seen that the position of the pulsation bubble generally coincides with the position of the shear zone.

In essence, the previous analysis has shown that in the wheel wake as well as in the shear zone, mechanisms related to wheel rotation have a predominant effect in the observation zone located near the ground. Both the ventilation effects and the rotation effects are most pronounced, which is clearly visible in the SPOD spectrum, as well as in the range of the corresponding coherent structures (and their maximum amplitudes). As for all the other effects (e.g. shear induced pulsations), their range and origin are not immediately clear and may require additional studies to be directly identified, although it can be inferred that some connection with the shearing of the ring vortices in the wheel wake can be drawn.

CONCLUSIONS

In this work, the SPOD algorithm is used for the identification of energetically coherent structures in the wake of the rotating car wheel. Source data have been collected from the experimental campaign involving 2D high-speed PIV measurements in the zone around the wake of the rotating wheel. Effects related to wheel rotation have been identified as the most energetic feature of the flow, including the ventilation effect and wheel rotation. Other effects related to shear are also visualized. The presented analysis provides insight into the dynamics of coherent structures in the wheel wake and identifies their dominant features. Future work in this direction should include the analysis of measurement results at different heights as well as in an enlarged observation window in order to provide a clearer understanding of the dominant physical mechanisms in the vehicle wake.

Acknowledgments. The authors gratefully acknowledge the Research Association of Automotive Technology (Forschungsvereinigung Automobiltechnik e.V. - FAT) and the Working Group 6 ‘Aerodynamics’ (Arbeitskreis 6 ‘Aerodynamik’) for supporting this project dealing with ‘Characterization and simulation of wheel flow during real tire deformation’ (‘Charakterisierung und Simulation der Radumströmung bei realer Reifendeformation’).

REFERENCES

Matsumoto, Daiki, Nakae, Yusuke, Niedermeier, Christoph, Tanaka, Hiroshi & Indinger, Thomas 2019 Application of dynamic mode decomposition to influence the driving stability of road vehicles. In *WCX SAE World Congress Experience*. SAE International.

Mrosek, Markus & Othmer, Carsten 2019 Reduced-order modeling of vehicle aerodynamics via proper orthogonal decomposition. *SAE International Journal of Passenger Cars - Mechanical Systems* **12** (3), 225–236.

Schmidt, Oliver & Colonius, Tim 2020 Guide to spectral proper orthogonal decomposition. *AIAA journal* **58** (3), 1023–1033.

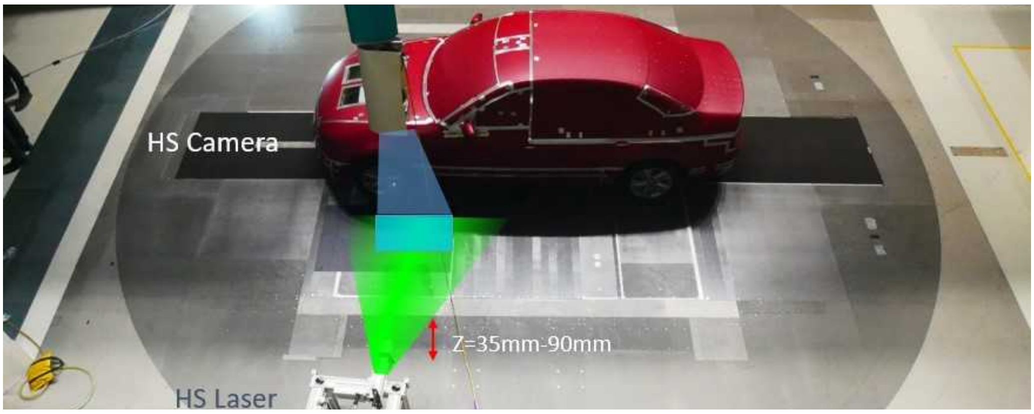

Figure 1. Arrangement of the experimental setup, with the observation zone indicated, positioned near the front left wheel.

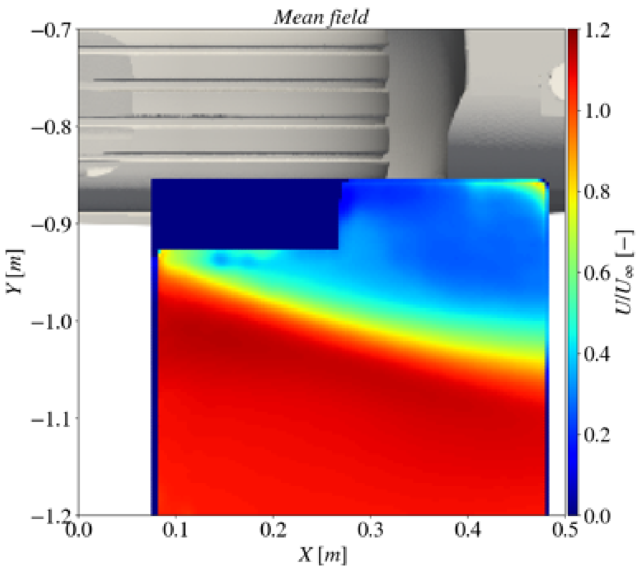

Figure 2. Mean velocity field in the observation zone. Detail in the background shows the silhouette of the car, with tire grooves

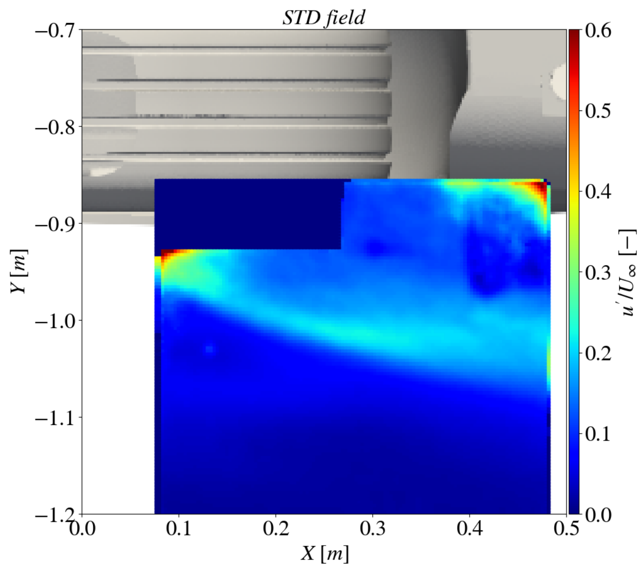

Figure 3. Field of the standard deviation of velocity fluctuations in the observation zone. Detail in the background shows the silhouette of the car, with tire grooves.

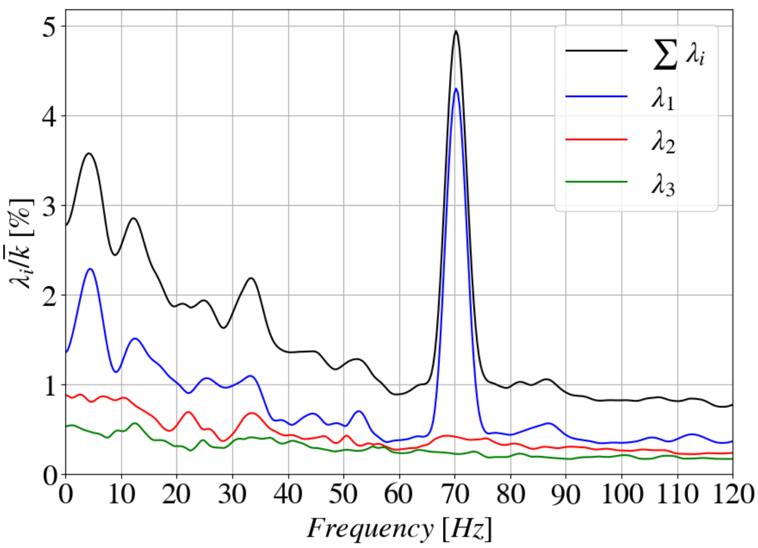

Figure 4. Eigenvalues for three leading SPOD modes, as well as the power spectral density along the entire spectrum (plotted in black). All the values are scaled by the turbulent kinetic energy k

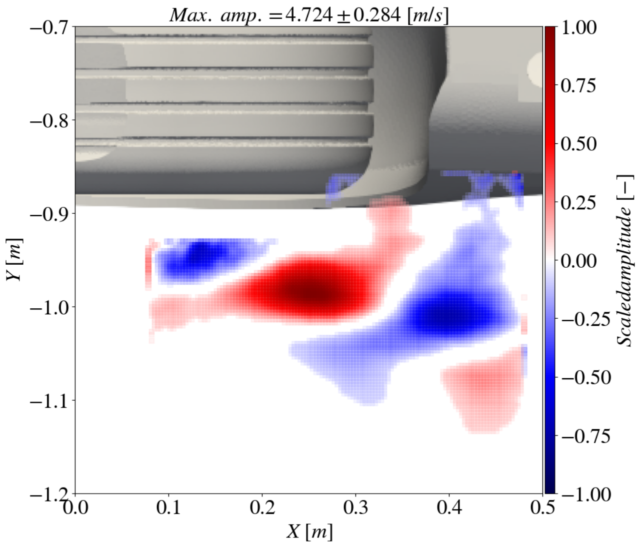

Figure 5. Reconstructed pulsation of the velocity field, from the mode oscillating at $f = 70\ Hz$.

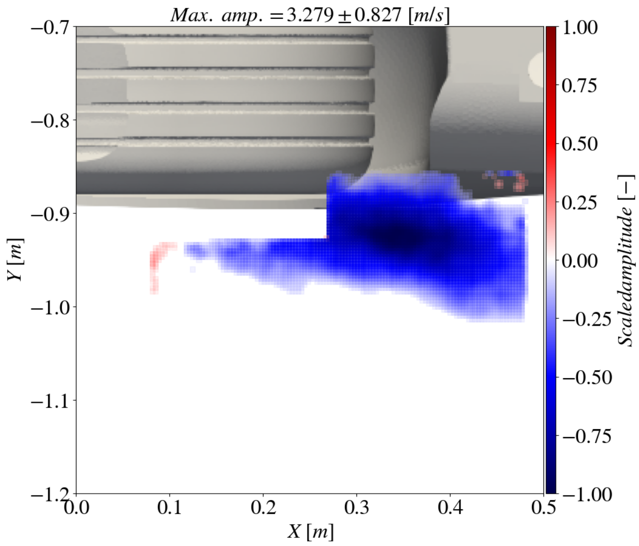

Figure 6. Reconstructed pulsation of the velocity field, from the mode oscillating at $f = 6\ Hz$.

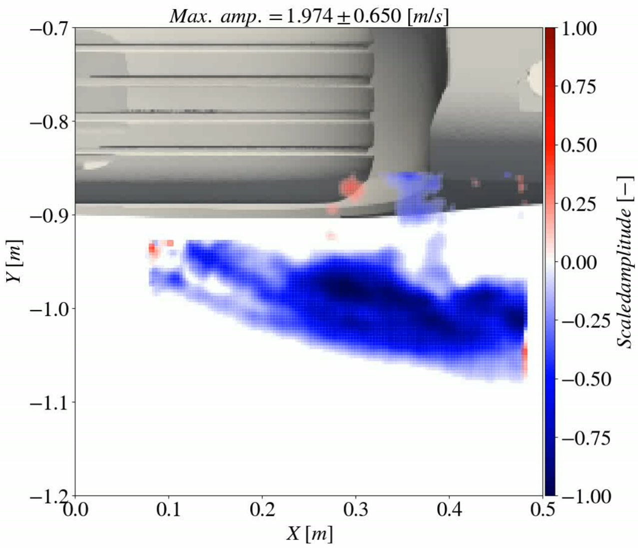

Figure 7. Reconstructed pulsation of the velocity field, from the mode oscillating at $f = 14\ Hz$.

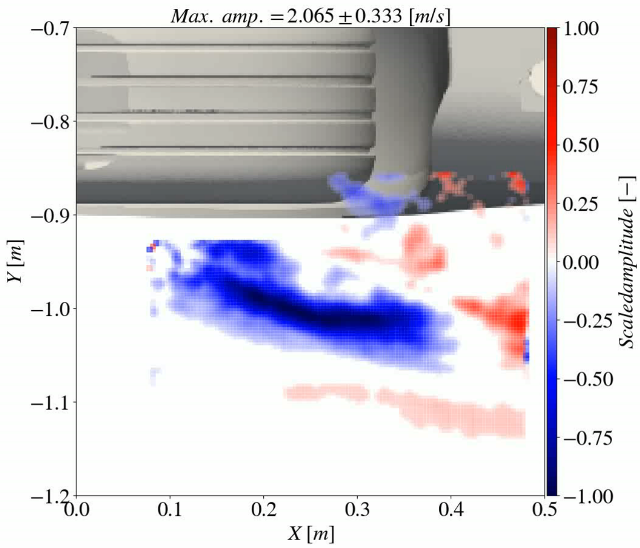

Figure 8. Reconstructed pulsation of the velocity field, from the mode oscillating at $f = 32\ Hz$.